Quantum geometry quadrupole-induced third-order nonlinear transport in antiferromagnetic topological insulator $MnBi_2Te_4$

Hui Li[1#], Chengping Zhang[1#], Chengjie Zhou[1], Chen Ma[1], Xiao Lei[2], Zijing Jin[1], Hongtao He[2], Baikui Li[1], Kam Tuen Law[1]*, Jiannong Wang[1]*

[1]*Department of Physics, the Hong Kong University of Science and Technology, Clear Water Bay, Hong Kong, China*

[2]*Department of Physics, South University of Science and Technology of China, Shenzhen, Guangdong 518055, China*

[#]These authors contributed equally to this work.

*Correspondence and requests for materials should be addressed to K. T. L. (email: phlaw@ust.hk), and J. W. (email: phjwang@ust.hk).

Supplementary Note 1. Atomic force image of the $MnBi_2Te_4$ flakes

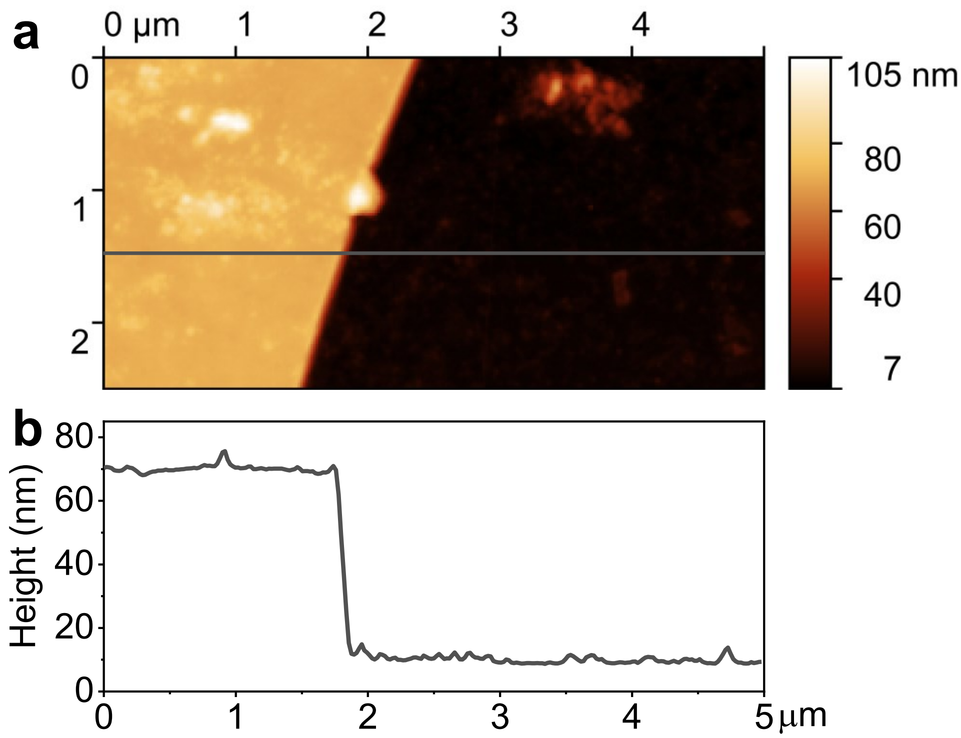

Supplementary Fig. 1 Atomic force image of the $MnBi_2Te_4$ flakes. The thickness of $MnBi_2Te_4$ flake is determined to be ~60 nm.

Supplementary Note 2. Ohmic contact and consistency of third-harmonic nonlinear response

We have measured the two-terminal *I-V* curves of the devices, as shown in Fig. S2(b). As can be seen, all the *I-V* curves measured between the two probes of bulk $MnBi_2Te_4$ marked in Fig. S2(a) are of linear characteristic, which suggests the devices are of good ohmic contact.

We further measured the third-harmonic nonlinear Hall voltage for two pairs of Hall bar, as shown in Fig. S2(c). The cyan curve is collected between the Hall bar probes 5-6 and is compared to the previous measurement presented in the main text (purple curve). The orange curve is measured between the Hall bar probes 3-4. As can be seen, the overall features of the sharp transitions along with the magnetization transition of the bulk $MnBi_2Te_4$ are well reproducible. These results demonstrate a good consistency and reproducibility of the nonlinear transport measurements in our work.

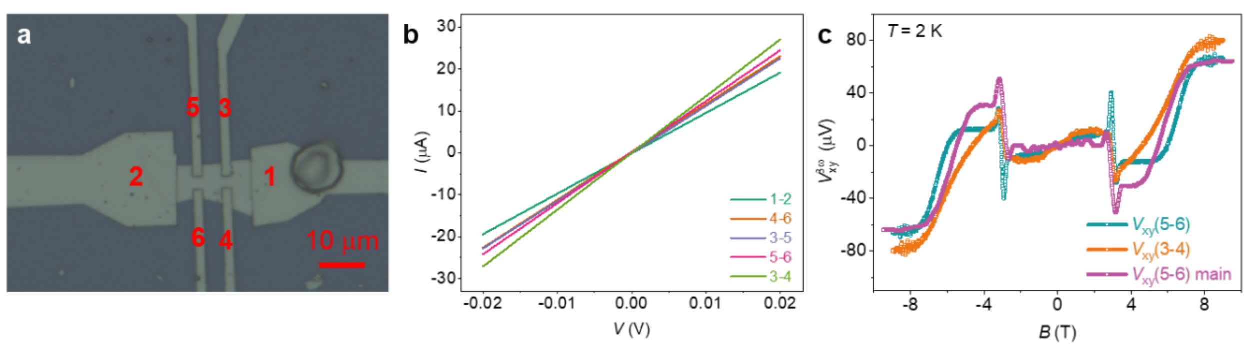

Supplementary Fig. 2. (a) Optical image of the bulk $MnBi_2Te_4$ devices. Six electrodes are patterned on the bulk $MnBi_2Te_4$ flakes with the number of electrodes being indicated. (b) Two-terminal *I-V* curves of the devices measured between different probes indicated. (c) Third-harmonic nonlinear Hall voltage as a function of the out-of-plane magnetic fields. The cyan and orange curves are measured from the different Hall bar indicated. The purple curve is adopted from the main text and was measured between the same Hall bar probes as that of cyan curve.

Supplementary Note 3. Nonlinear *I-V* characteristic of $MnBi_2Te_4$ flakes and resistor

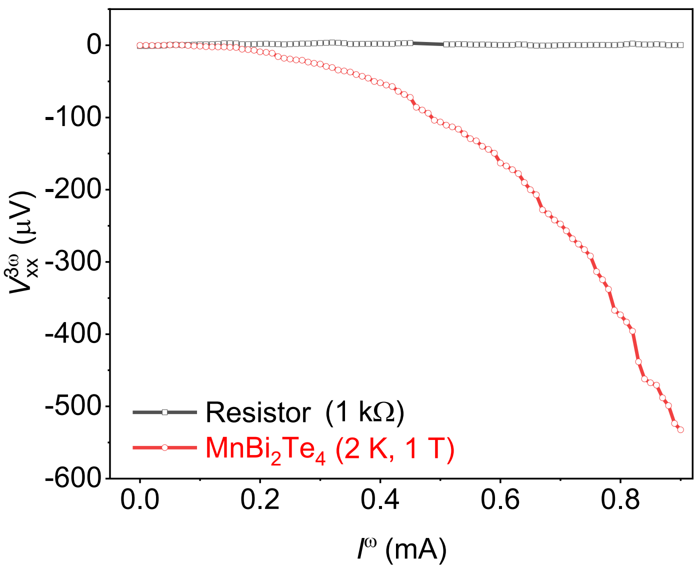

Supplementary Fig. 3 Nonlinear *I-V* curves of $MnBi_2Te_4$ flakes and resistor. Third-harmonic longitudinal voltage as a function of first-harmonic current for $MnBi_2Te_4$ (red curve, 2 K and 1 T) and the resistor of 1 kΩ (black curve, 0 T).

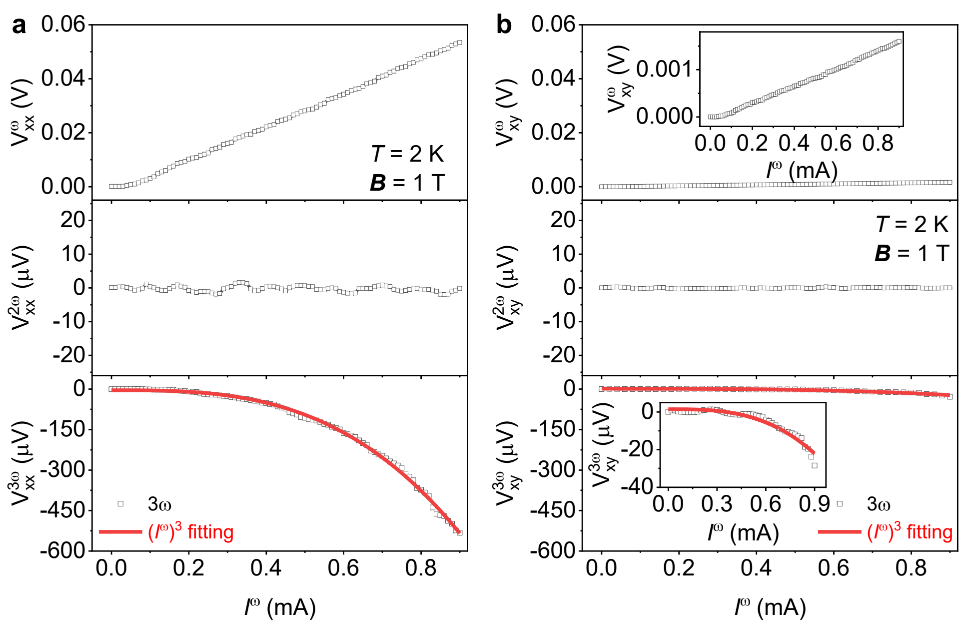

Supplementary Fig. 4 *I-V* curves of $MnBi_2Te_4$ flakes at different harmonics. First- (top panel), Second- (middle panel) and Third-harmonic longitudinal (a) and transverse (b) voltage as a function of first-harmonic current for $MnBi_2Te_4$ measured at $T = 2$ K and $\boldsymbol{B} = 1$ T. The red curve in the bottom panels is the fitting result following the relationship of $V^{3\omega} \propto (I^{\omega})^3$.

Supplementary Note 4. Frequency dependent of the third-harmonic nonlinear response

We have measured the frequency dependent third-harmonic nonlinear *I-V* characteristic of bulk $MnBi_2Te_4$ flakes ranging from 73 Hz to 733 Hz for both longitudinal (Fig. S5a) and transverse (Fig. S5b) directions at 2 K and 9 T. As can be seen, all the curves collected at different frequencies are well overlapped, suggesting the nonlinear response of the $MnBi_2Te_4$ flakes is independent of the frequency of driving current.

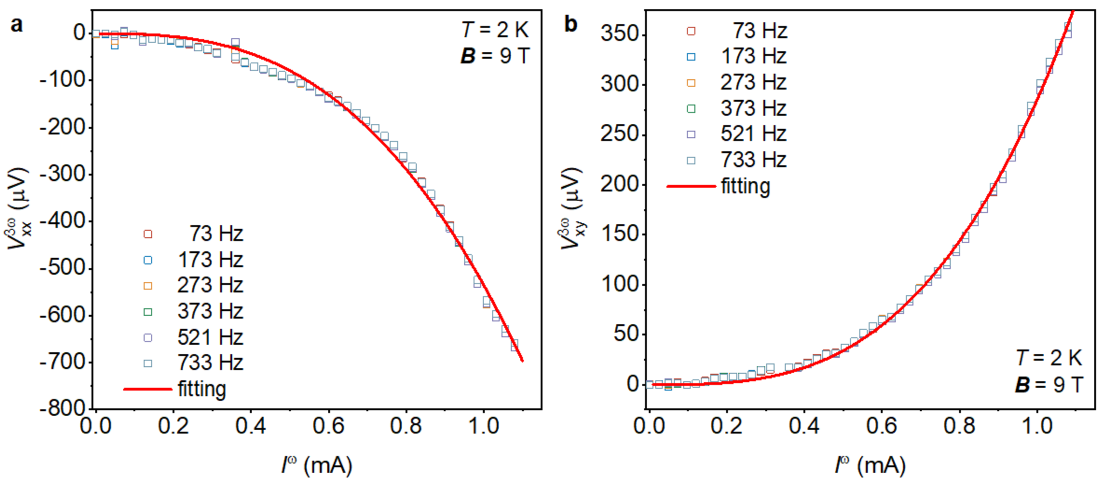

Supplementary Fig. 5. Third-harmonic nonlinear *I-V* characteristic curves of $MnBi_2Te_4$ flakes along longitudinal (a) and transverse (b) direction measured at different frequencies indicated. The red lines are the fitting curves.

Supplementary Note 5. Driving current dependence of the first- and third-harmonic resistance/voltage

We have measured the temperature and magnetic field dependence of the first-harmonic and third-harmonic longitudinal and transverse resistance/voltage under different driving currents of 0.3 mA (black curve) and 0.6 mA (red curve), respectively.

As shown in Fig. S6(a) and Fig. S6(b) below, the T_N of bulk $MnBi_2Te_4$ changed very little with increasing driving current from 0.3 mA to 0.6 mA. The switching field of the magnetization transitions of bulk $MnBi_2Te_4$ is almost the same with increasing driving current, as evidenced by the magnetic field dependences of the first-harmonic longitudinal resistance (Fig.S6(c)) and Hall resistance (Fig. S6(e)) and the third-harmonic longitudinal scaling factor $\frac{V_{xx}^{3\omega}}{(V_{xx}^{\omega})^3}$ (Fig. S6(d)) and transverse scaling factor $\frac{V_{xy}^{3\omega}}{(V_{xx}^{\omega})^3}$ (Fig. S6(f)).

Generally, the heating effect could amplify the magnitude of the high-order nonlinear signal. When the applied current in the measurements is reduced from 0.6 mA to 0.3 mA, the heating effect is supposed to be reduced. In this case, the smaller $\frac{V_{xx}^{3\omega}}{(V_{xx}^{\omega})^3}$ and $\frac{V_{xy}^{3\omega}}{(V_{xx}^{\omega})^3}$ ratio is expected to be obtained at lower driving current. However, as shown in Fig. S6b, 6d and 6f, we observed a higher $\frac{V_{xx}^{3\omega}}{(V_{xx}^{\omega})^3}$ and $\frac{V_{xy}^{3\omega}}{(V_{xx}^{\omega})^3}$ ratio for the smaller driving current of 0.3 mA (black curve). This discrepancy validates the experimental observations are related to the quantum geometry effect of bulk $MnBi_2Te_4$ rather than stemming from the heating effect.

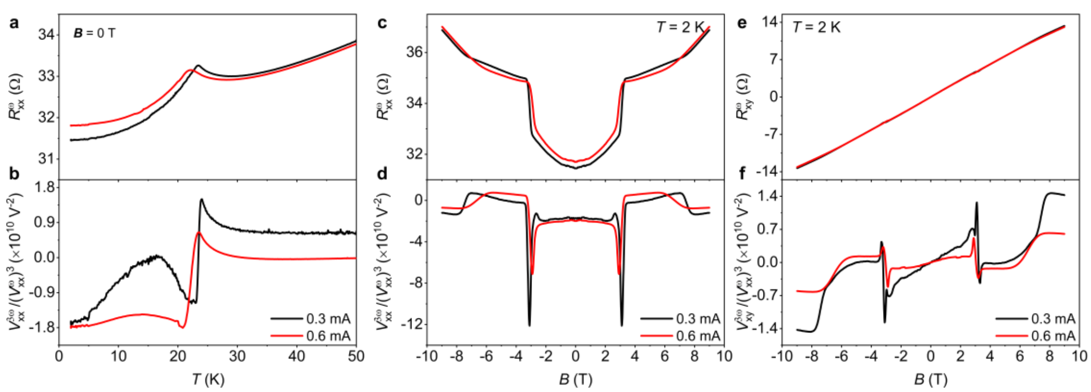

Supplementary Fig. 6 Transport properties of bulk $MnBi_2Te_4$ under different driving current. First-harmonic longitudinal resistance (a) and third-harmonic longitudinal scaling factor $\frac{V_{xx}^{3\omega}}{(V_{xx}^{\omega})^3}$ (b) of bulk $MnBi_2Te_4$ as a function of temperature measured under 0.3 mA (black curve) and 0.6 mA (red curve), respectively. Magnetic field dependent of first-harmonic longitudinal resistance (c), third-harmonic longitudinal scaling factor $\frac{V_{xx}^{3\omega}}{(V_{xx}^{\omega})^3}$ (d), first-harmonic Hall resistance (e) and third-harmonic transverse scaling factor $\frac{V_{xy}^{3\omega}}{(V_{xx}^{\omega})^3}$ (f) collected under 0.3 mA (black curve) and 0.6 mA (red curve), respectively.

Supplementary Note 6. Magnetotransport properties of $MnBi_2Te_4$ flakes

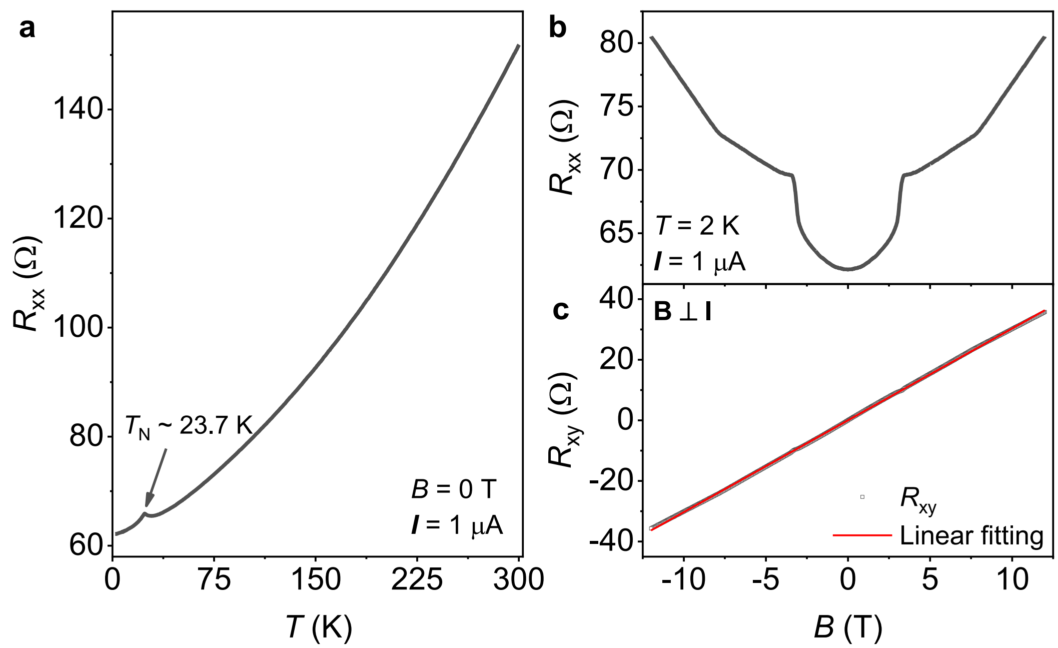

Supplementary Fig. 7 Magnetotransport properties of $MnBi_2Te_4$ flakes. (a) Temperature dependent longitudinal resistance (R_{xx}) of $MnBi_2Te_4$ flakes at B = 0 T. The magnitude of measured direct current is set at 1 μA. The ***B***-field dependence of longitudinal resistance (R_{xx}) (b) and transverse resistance (R_{xy}) (c) of $MnBi_2Te_4$ flakes measured at T = 2 K and I = 1 μA. The carrier density is calculated to be ~ 2.06×10^{19} cm^{-3} from the linear fitting of R_{xy}.

Supplementary Note 7. Raw data of the third-harmonic voltages of $MnBi_2Te_4$ flakes

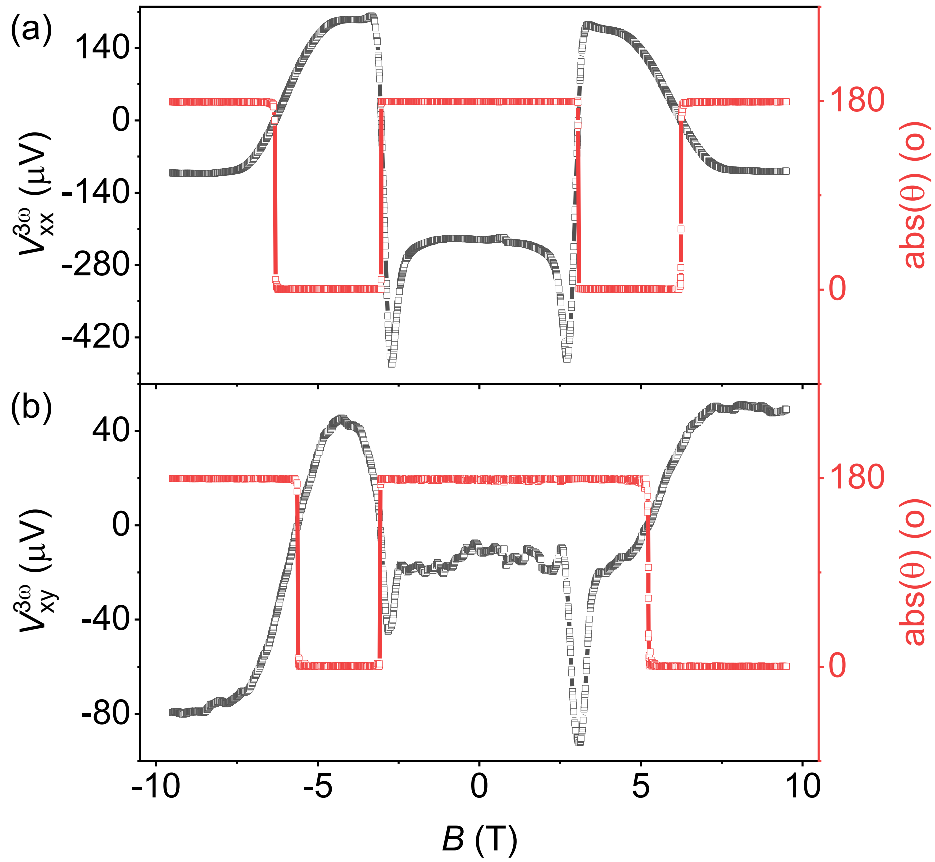

Supplementary Fig. 8 B-fields dependent third-harmonic voltages of $MnBi_2Te_4$ flakes. B-fields dependence of $V_{xx}^{3\omega}$(a) and $V_{xy}^{3\omega}$(a) of $MnBi_2Te_4$ flakes measured at T = 2 K and I_{AC} = 0.6 mA. The red curves indicate the absolute value of phase for the third-harmonic voltages along with the **B**-fields.

Supplementary Note 8. Theoretical calculations

In this section, we provide the details of the effective Hamiltonian of $MnBi_2Te_4$ flakes in our theoretical calculations with a magnetic order Δ induced by the external magnetic field. As mentioned in the Methods section of the main text, the effective Hamiltonian reads

$$\mathcal{H}(\boldsymbol{k}) = \mathcal{H}_0(\boldsymbol{k}) + \Delta\, \mathcal{H}_{\mathrm{M}}(\boldsymbol{k}) \qquad \text{(Eq. S1)}$$

where

$$\mathcal{H}_0(\boldsymbol{k}) = \epsilon_0(k) + \begin{pmatrix} M_\gamma(k) & A_1 k_z & 0 & A_2 k_- \\ A_1 k_z & -M_\gamma(k) & A_2 k_- & 0 \\ 0 & A_2 k_+ & M_\gamma(k) & -A_1 k_z \\ A_2 k_+ & 0 & -A_1 k_z & -M_\gamma(k) \end{pmatrix}$$

is the term which preserves the $\mathcal{PT}$ symmetry, and

$$\mathcal{H}_M(\boldsymbol{k}) = \begin{pmatrix} M_1(k) & A_3 k_z & 0 & A_4 k_- \\ A_3 k_z & M_2(k) & -A_4 k_- & 0 \\ 0 & -A_4 k_+ & -M_1(k) & A_3 k_z \\ A_4 k_+ & 0 & A_3 k_z & -M_2(k) \end{pmatrix}$$

is the part which breaks the time-reversal symmetry.

The basis of the Hamiltonian is $\{|P1_z^+,\uparrow\rangle,\ |P2_z^-,\uparrow\rangle,\ |P1_z^+,\downarrow\rangle,\ |P2_z^-,\downarrow\rangle,\}$. Here, $k_\pm = k_x \pm i k_y$, $\epsilon_0(k) = C + D_1 k_z^2 + D_2(k_x^2 + k_y^2)$, $M_\gamma(k) = M_0^\gamma + B_1^\gamma k_z^2 + B_2^\gamma(k_x^2 + k_y^2)$, $M_{1,2}(k) = M_\alpha(k) \pm M_\beta(k)$, and $M_j(k) = M_0^j + B_1^j k_z^2 + B_2^j(k_x^2 + k_y^2)$ with $j = \alpha, \beta$. The parameters for $\mathcal{H}(\boldsymbol{k})$ are adapted from Ref. [1] in the main text and listed in Table.SI.

TABLE SI. Parameters for the effective Hamiltonian $\mathcal{H}(\boldsymbol{k})$ of the $MnBi_2Te_4$ flakes adapted from Ref. [1] in the main text.

C(eV)	D_1(eVÅ^2)	D_2(eVÅ^2)	M_0^γ(eV)	B_1^γ(eVÅ^2)	B_2^γ(eVÅ^2)	A_1(eVÅ)	A_2(eVÅ)
0.0539	-4.0339	4.4250	0.0307	4.2857	8.3750	1.3658	1.9985
M_0^α(eV)	B_1^α(eVÅ^2)	B_2^α(eVÅ^2)	M_0^β(eV)	B_1^β(eVÅ^2)	B_2^β(eVÅ^2)	A_3(eVÅ)	A_4(eVÅ)
-0.1078	0.6232	0.6964	-0.0880	2.7678	1.9650	-0.5450	1.1384

Supplementary Note 9. Scaling law analysis of the third-harmonic nonlinear voltages

Scaling law analysis of the third-harmonic longitudinal nonlinear voltages

The C_3 symmetry of $MnBi_2Te_4$ crystal requires the third-harmonic nonlinear ***longitudinal*** conductivity can only come from the quantum metric quadrupole and Drude contributions, while the third-order ***Hall*** conductivity is only contributed by Berry curvature quadrupole (BCQ) and skew scattering. The quantum metric quadrupole and the Drude contribution have different dependence on the scattering time τ. Therefore, we can distinguish them with the scaling law analysis, as the reviewer suggested in the next question.

The third-order nonlinear conductivity contributed by the quantum metric quadrupole is $j_{x,QMQ}^{3\omega} = \frac{e^4\tau}{\hbar^2} G_{xxxx} E_x^3$, where $G_{xxxx} = -\int_{\boldsymbol{k}} \partial_x^2 G_{xx} f_0 + \frac{1}{2}\int_{\boldsymbol{k}} v_x^2 G_{xx} f_0''$ can be expressed as the integral of the quantum metric quadrupole $\partial_x^2 G_{xx}$ and the (normalized) quantum metric G_{xx}. Recall the linear conductivity from the Drude formula $\sigma_{xx} = \frac{ne^2\tau}{m_{eff}}$, we get the relation between the third-harmonic longitudinal voltage $V_{x,QCQ}^{3\omega}$ and the driving ac voltage $(V_x^{\omega})^3$ as

$$\frac{V_{x,QCQ}^{3\omega}}{(V_x^{\omega})^3} = \frac{1}{L^2}\frac{e^2 m_{eff}}{\hbar^2 n} G_{xxxx} \qquad \text{(Eq. S2)}$$

where L, e, m_{eff}, $\hbar$, and n are the length between the voltage probes, elemental charge, effective mass, reduced Plank constant, and carrier density, respectively. Eq. S2 clearly shows that the quantum metric quadrupole induced third-harmonic nonlinear longitudinal voltage is ***independent of the scattering time*** $\boldsymbol{\tau}$ or the longitudinal conductivity σ_{xx}.

On the other hand, the Drude contribution to the third-order longitudinal current is $j_{x,D}^{3\omega} = \frac{e^4\tau^3}{\hbar^4} D_{xxxx} E_x^3$ with $D_{xxxx} = \int_{\boldsymbol{k}} \partial_x^4 \varepsilon(k) f_0$, which yields the third-harmonic nonlinear longitudinal voltage,

$$\frac{V_{x,D}^{3\omega}}{(V_x^{\omega})^3} = \frac{1}{L^2}\frac{m_{eff}^3 D_{xxxx}}{e^2\hbar^4 n^3}\sigma_{xx}^2 \qquad \text{(Eq. S3)}$$

Together, we obtain the total third-harmonic nonlinear longitudinal voltage,

$$\frac{V_x^{3\omega}}{(V_x^{\omega})^3} = \frac{1}{L^2}\frac{m_{eff}^3 D_{xxxx}}{e^2\hbar^4 n^3}\sigma_{xx}^2 + \frac{1}{L^2}\frac{e^2 m_{eff}}{\hbar^2 n} G_{xxxx} = \alpha\sigma_{xx}^2 + \beta \qquad \text{(Eq. S4)}$$

Therefore, the slope α is directly related to the Drude-like contribution, while the intercept β characterizes the quantum metric quadrupole contribution.

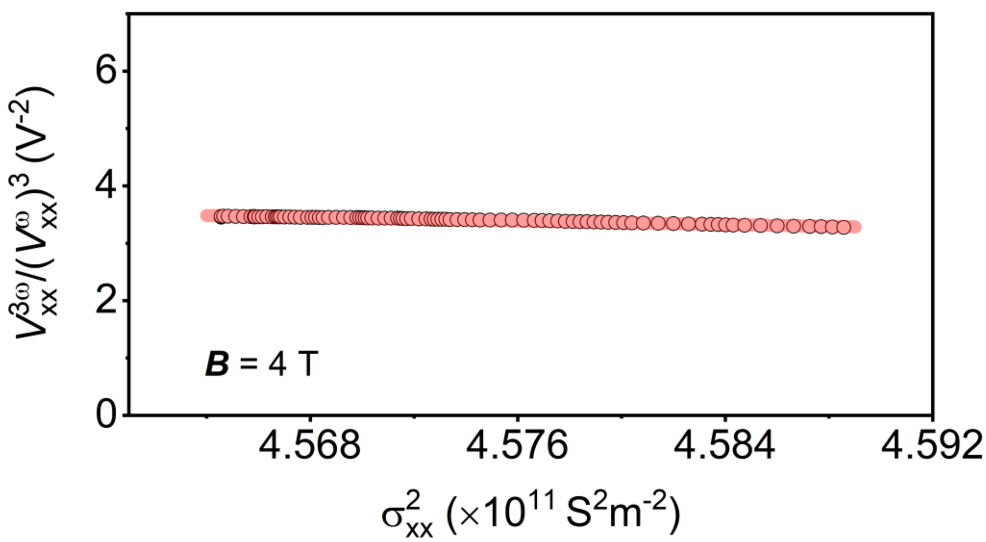

Supplementary Fig. 9 The nonlinear longitudinal voltage $\frac{V_{xx}^{3\omega}}{(V_{xx}^{\omega})^3}$ as a function of square of the linear conductivity σ_{xx}^2 at $\boldsymbol{B}$ = 4 T and T < 10 K for bulk $MnBi_2Te_4$. The red line is the linear fitting curve.

The fitting of Eq. S4 to the experimental data is shown in Fig. S9 and yields $\alpha = (-7.91 \times 10^{-11} \pm 1.01 \times 10^{-12})\, V^{-2}\Omega^2\mathrm{m}^2$ and $\beta = (39.58 \pm 0.46)\, V^{-2}$. At low temperatures with $\sigma_{xx} = 6.76 \times 10^5\, S/m$, we find the Drude-like contribution $\alpha\sigma_{xx}^2 = -36.11\, V^{-2}$ is comparable with the quantum metric quadrupole contribution $\beta = 39.58\, V^{-2}$.

Scaling law analysis of the third-harmonic transverse nonlinear voltages

For the ***Hall response*** (the voltage perpendicular to the driving current), the third-order Hall conductivity can only be contributed by the Berry curvature quadrupole (BCQ) and skew scatterings due to the C_3 symmetry of $MnBi_2Te_4$ crystal.

The third-order nonlinear anomalous Hall effect contributed by the Berry curvature quadrupole Q_{xxz} is $j_{y,BCQ}^{3\omega} = \frac{e^4\tau^2}{\hbar^3} Q_{xxz} E_x^3$. Recall the linear conductivity from the Drude formula $\sigma_{xx} = \frac{ne^2\tau}{m_{eff}}$, we get the third-harmonic Hall voltage

$$\frac{V_{y,BCQ}^{3\omega}}{(V_x^{\omega})^3} = \frac{W}{L^3}\frac{m_{eff}^2}{\hbar^3 n^2}\mathcal{Q}_{xxz}\sigma_{xx} \quad \text{(Eq. S5)}$$

where W, L, e, m_{eff}, $\hbar$, and n are the width of the device, the length between the voltage probes, elemental charge, effective mass, reduced Plank constant, and carrier density, respectively.

On the other hand, the skew scattering induced third-order nonlinear anomalous Hall current reads

$$j_{y,sk}^{3\omega} = -e\int dk\, v_y(k) f_A^{(3)}(k) \quad \text{(Eq. S6)}$$

where $v_y(k) = \frac{1}{\hbar}\partial_y \varepsilon(k)$ is the group velocity, and $f_A^{(3)}(k)$ is the third-order correction to the Fermi-Dirac distribution function by skew scattering. $f_A^{(3)}(k)$ can be estimated as $f_A^{(3)}(k) \sim \frac{\tau}{\bar{\tau}}\frac{e^3\tau^3}{\hbar^3}\partial_x^3 f_0 E_x^3$ [2], where $\bar{\tau}$ is the skew scattering time, which yields the nonlinear Hall voltage

$$\frac{V_{y,sk}^{3\omega}}{(V_x^{\omega})^3} \sim \frac{W}{L^3}\frac{m_{eff}^2}{2e^4 n^3 \varepsilon_F \bar{\tau}}\sigma_{xx}^3 \quad \text{(Eq. S7)}$$

Together, we obtain the total third-harmonic nonlinear Hall voltage

$$\frac{V_y^{3\omega}}{\sigma_{xx}(V_x^{\omega})^3} = \frac{W}{L^3}\frac{m_{eff}^2}{2e^4 n^3 \varepsilon_F \bar{\tau}}\sigma_{xx}^2 + \frac{W}{L^3}\frac{m_{eff}^2}{\hbar^3 n^2}\mathcal{Q}_{xxz} = \eta\sigma_{xx}^2 + \xi \quad \text{(Eq. S8)}$$

where we have divided the nonlinear Hall voltage with a factor of σ_{xx} for the benefit of the fitting.

The fitting of Eq. S8 to the experimental data is shown in Fig. S10 and yields $\eta = (5.79 \times 10^{-17} \pm 9.32 \times 10^{-19})\ V^{-2}\Omega^3\mathrm{m}^3$ and $\xi = (-2.73 \times 10^{-5} \pm 4.26 \times 10^{-7})\ \mathrm{V}^{-2}\Omega\mathrm{m}$. Considering $\sigma_{xx} = 6.76 \times 10^5\ S/m$ at low temperatures, we find the skew scattering contribution $\eta\sigma_{xx}^3 = 17.88\ V^{-2}$ is comparable with the Berry curvature quadrupole contribution $\xi\sigma_{xx} = -18.45\ V^{-2}$.

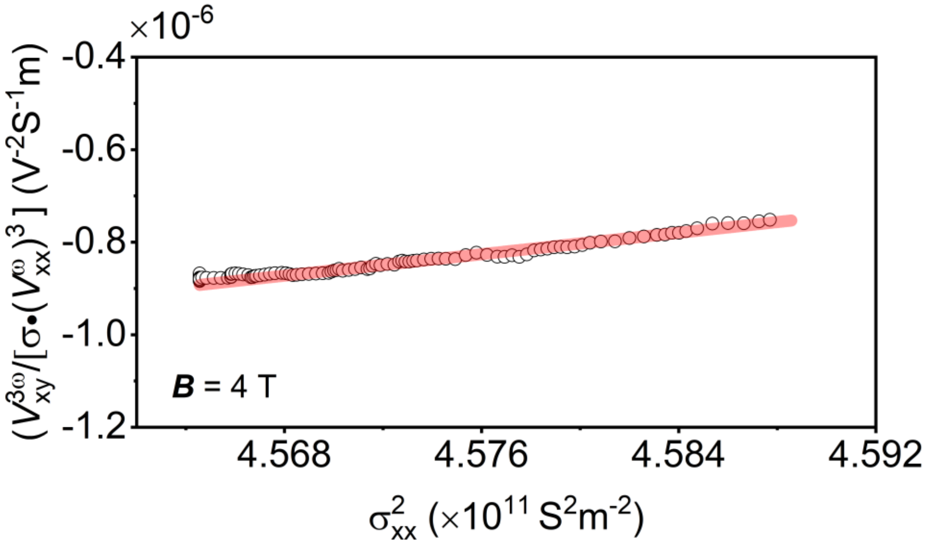

Supplementary Fig. 10 The nonlinear transverse voltage $\frac{V_{xy}^{3\omega}}{\sigma_{xx}(V_{xx}^{\omega})^3}$ as a function of square of the linear conductivity σ_{xx}^2 at $\boldsymbol{B}$ = 4 T and T < 10 K for bulk $MnBi_2Te_4$. The red line is the linear fitting curve.

References

1. Zhang, D., Shi, M., Zhu, T., Xing, D., Zhang, H., & Wang, J., Topological axion states in the magnetic insulator $MnBi_2Te_4$ with the quantized magnetoelectric effect, *Phys. Rev. Lett.* **122,** 206401 (2019).
2. Isobe, H., Xu, S.-Y., & Fu, L., High-frequency rectification via chiral Bloch electrons. *Sci. Adv.* **6**, eaay2497(2020).